ESANN 2017 proceedings, European Symposium on Artificial Neural Networks, Computational Intelligence and Machine Learning. Bruges (Belgium), 26-28 April 2017, i6doc.com publ., ISBN 978-287587039-1.
Available from http://www.i6doc.com/en/.

Hyper-spectral frequency selection for the classification of vegetation diseases

K. Dijkstra[1,2], J. van de Loosdrecht[1], L.R.B. Schomaker[2] and M.A. Wiering[2]

1- NHL University of Applied Sciences
Centre of Expertise in Computer Vision
P.O. Box 1080, 8900 CB, Leeuwarden. Netherlands.

2- University of Groningen
Institute of Artificial Intelligence and Cognitive Engineering
PO Box 407, 9700 AK, Groningen. Netherlands.

Abstract. Reducing the use of pesticides by early visual detection of diseases in precision agriculture is important. Because of the color similarity between potato-plant diseases, narrow band hyper-spectral imaging is required. Payload constraints on unmanned aerial vehicles require reduction of spectral bands. Therefore, we present a methodology for per-patch classification combined with hyper-spectral band selection. In controlled experiments performed on a set of individual leaves, we measure the performance of five classifiers and three dimensionality-reduction methods with three patch sizes. With the best-performing classifier an error rate of 1.5% is achieved for distinguishing two important potato-plant diseases.

1 Introduction

The Netherlands has a leading role in the cultivation and export of seed potatoes, mainly due to their high quality. Monitoring quality and optimizing crop yield are therefore important. Agricultural fields are regularly checked for diseased plants, which are prevented or counteracted using pesticides.

Many types of leaf damages can occur, varying from environmental effects [1] to fungal infections. When a disease is incorrectly diagnosed, a wrong treatment could be chosen. For example, pesticides are applied while there is no fungal infection. This could have a negative impact on the environment or even promote resistance to pesticides.

Two commonly-confused damages on potato plants are caused by either an *Alternaria* fungal infection or by exposure to ozone (O^3) [2]. Both produce similar brownish lesions on the leaf (Figure 1). *Alternaria* should be treated with pesticides while ozone damage should not. This makes a correct diagnosis important.

Unmanned Aerial Vehicles (UAVs) are popular for monitoring agricultural fields [3]. Examples are vegetation index calculation [4], crop recognition [5] and disease detection [6]. These applications often use commodity multi-spectral cameras which only measure Blue, Green, Red, Red Edge and Near Infrared spectral wavelengths. These sensors are not particularly suitable for detecting subtle color differences in potato leaf lesions because of their broad spectral sensitivity and limited spectral resolution.

ESANN 2017 proceedings, European Symposium on Artificial Neural Networks, Computational Intelligence and Machine Learning. Bruges (Belgium), 26-28 April 2017, i6doc.com publ., ISBN 978-287587039-1.
Available from http://www.i6doc.com/en/.

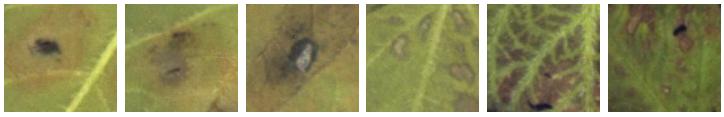

Fig. 1: *Alternaria* damage (left three images) and ozone damage (right three images).

The goal of this research is to develop a methodology for distinguishing between two similarly looking diseases. Hyper-spectral images of potato leaves are created. From this image cube a subset of wavelengths is determined which can be recorded by UAVs with limited payload. Several common and state-of-the-art classification algorithms are tested on this dataset to determine the impact of low dimensional projections on the per-pixel classification error rates.

2 Materials and Methods

Images of individual leaves are taken in a controlled environment on a dark background. The imaging system consists of a high resolution camera and a liquid crystal tunable filter. The camera has a sensor diagonal of 1", a resolution of 2000 x 2000 pixels and 12 bits gray-scale pixel depth. The filter is adjusted to 28 wavelengths from 450nm to 720nm with 10nm intervals and 10nm bandwidth.

A ground-truth set is created by a trained expert under laboratory conditions. It consists of 5 leaves with *Alternaria* damage and 5 with ozone damage. The damages were verified with a separate biological test. A per-pixel reference is hand painted over the original image using ground-truth annotation software. A source sample is formed by making a pair of *Alternaria* and ozone leaves. From each of these five source samples 8000 random patches were picked: 4000 leaf, 2000 *Alternaria* and 2000 ozone, resulting in a total of 40000 samples. Three patch sizes are used: 1x1, 3x3 and 5x5 pixels. Because a patch of the hyper-spectral data cube is three dimensional the maximum dimensionality is 5 x 5 x 28 = 700. A relatively high amount of samples were chosen because of the high dimensionality of the data.

2.1 Hyper-spectral normalization and sample selection

The camera-sensor response, the wavelength-dependent filter response and inhomogeneous illumination result in distorted images. A per-pixel normalization is performed by dividing each intensity with the background intensity (i.e. an image containing no leaf).

$$\begin{aligned} w \in \quad & \{450nm, 460nm, 470nm, ..., 720nm\} \\ I^w = \quad & \frac{I^w_{raw}}{I^w_{bg}+k} \quad , \end{aligned}$$

where w is one of the 28 spectral wavelengths, I^w_{bg} is the background image, I^w_{raw} and I^w are the raw image and corrected image, k is a small constant to avoid

ESANN 2017 proceedings, European Symposium on Artificial Neural Networks, Computational Intelligence and Machine Learning. Bruges (Belgium), 26-28 April 2017, i6doc.com publ., ISBN 978-287587039-1.
Available from http://www.i6doc.com/en/.

dividing by zero.

Random patches are drawn from a sample with respect to its class using:

$$\begin{aligned} c &\in \{Leaf, Alternaria, Ozone\} \\ r &\in \{0, 1, 2\} \\ f(x, y, w, r, c) &= \{I^w(x-r, y-r)..I^w(x+r, y+r) \mid C(x, y) = c\}, \end{aligned}$$

where w is a wavelength, x, y, w is a location within the hyper-spectral image cube, r is half the side of a square patch, I is a source sample, C is the per-pixel reference image and c is the class to draw samples from.

2.2 Hyper-spectral frequency selection

Four linear projection methods are used for dimensionality reduction:

- *All*-projection uses the normalized intensities as input features: $w \in \{450nm, 460nm, 470nm, ..., 720nm\}$.
- *PCA*-projection uses the first three principal components: $w \in \{PC_1, PC_2, PC_3\}$. This is a common projection method which keeps the most relevant sources in the spectral bands.
- *LDA*-projection uses the linear discriminants: $w \in \{LD_1, LD_2\}$. This maximizes between-class variance and minimizes within-class variance, by projecting onto $nclasses - 1$ dimensions. This maximizes linear class separability.
- *3-Band*-projection selects three wavelengths which have the highest correlation with the linear discriminants calculated with the LDA-projection: $w \in \{520nm, 540nm, 680nm\}$. This is a powerful method to select individual spectral bands which contribute most to class separation. Also this projection does not need all 28 original bands and is therefore preferred for usage on a UAV.

The dimensionality when $r = 2$ (patch size is 5x5 pixels) is 700, 75, 50 and 75 for *All*, *PCA*, *LDA* and *3-Band*, respectively.

2.3 Classifying hyper-spectral image patches

Several classifiers are tested to investigate the impact of dimensionality reduction on the error rates. To get a fair estimate on the performance impact, several linear and non-linear classifiers are tested:

- *Gauss.* is a Gaussian density model using independent variables (Naive Bayes assumption). A sample is classified by calculating the likelihood for each dimension with respect to the class using a trained Gaussian model. By multiplying each likelihood the class with maximum likelihood is returned.
- *kNN* is a k-Nearest Neighbor classifier [7]. The value of k is experimentally determined to be 6 for optimal classification.
- *SVM* is a Support Vector Machine with a linear kernel [8].

ESANN 2017 proceedings, European Symposium on Artificial Neural Networks, Computational Intelligence and Machine Learning. Bruges (Belgium), 26-28 April 2017, i6doc.com publ., ISBN 978-287587039-1.
Available from http://www.i6doc.com/en/.

- *MLP_TanH* is a GPU accelerated Multilayer Perceptron (MLP) [9]. It uses a Hyperbolic Tangent transfer function, which is widely used for MLPs.
- *MLP_ReLU* is a GPU accelerated MLP with the faster ReLU transfer function ($x = max(0, x)$). A weight decay of 0.01 is used for regularization. Many state-of-the-art deep learning applications use a ReLU transfer function [9, 10].

Both MLP models use Stochastic Gradient Descent. The number of hidden units has been set to 4096, which was found to not over-fit the data and give the best performance. Furthermore, 100k iterations, a batch size of 200, a learning rate of 0.01 and a momentum of 0.1 are used for training. These values have been determined by manual experimentation.

2.4 Cascading classifiers

Classifying the image in several, increasingly difficult, stages makes evaluating the system easier. For example: First detect the leaf, then classify if there is damage and finally the disease which caused the damage. Error rates for per-pixel classifications are evaluated. In the future a final classification result should be produced by some kind of majority voting of all classified pixels of an image.

For this experiment, classifiers are trained on three classes (Healthy, Alternaria and Ozone). Leaf damage classification is separated from Alternaria/ Ozone disease classification. Error rates are calculated as if cascaded classifiers were used. $Error_{damage}$ is defined as the error with respect to the classified healthy and damaged leaf pixels. $Error_{disease}$ is the error with respect to Alternaria and Ozone classification.

3 Experiments and Results

Experiments have been performed with four projection methods, five classifiers and three patch sizes for a total of 60 experiments. Training is done with 32000 samples drawn from four source samples (each containing an image pair with either *Alternaria* or ozone damage). An additional 8000 samples are drawn from the fifth source sample for testing. This is repeated five times (once for each source sample). The average accuracy is reported.

Table 1 shows results for $error_{disease}$ for 3 patch sizes. Increasing patch size generally decreases error rates. Therefore results for $error_{damage}$ are only reported for the largest patch size (5x5). Testing speeds are reported in milliseconds (ms) on a Core I7-5820K CPU with a NVIDIA GTX 960 GPU.

For the disease classifier MLP_ReLU shows the lowest error (1.5%) when using all wavelengths. A standard PCA projection does not yield good classification results. With LDA projection, most classifiers show similarly low error rates (the best is 2.6%), which indicates a good choice for dimensionality reduction. This is further exploited by selecting three wavelengths which correlate best with the LDA projection. This increases the error rates from 1.5% to 7.3%, which still indicates an accuracy of 92.7%. Although kNN gives the lowest error rate when using only 3 wavelengths, MLP_ReLU seems the best overall choice

ESANN 2017 proceedings, European Symposium on Artificial Neural Networks, Computational Intelligence and Machine Learning. Bruges (Belgium), 26-28 April 2017, i6doc.com publ., ISBN 978-287587039-1. Available from http://www.i6doc.com/en/.

		$Error_{Disease}(\%)$			$Error_{Damage}(\%)$	
Model	Proj.	1x1 px	3x3 px	5x5 px	5x5 px	Time (ms)
MLP_ReLU	All	4.1	2.1	**1.5**	13.6	910
MLP_TanH		7.0	2.5	1.7	16.0	934
SVM		7.4	2.5	1.9	**13.4**	81,367
kNN		9.0	7.8	8.3	18.9	3,736,608
Gauss		23.7	23.5	27.4	49.7	1,491
MLP_ReLU	LDA	7.0	7.7	3.9	16.3	70
MLP_TanH		9.6	4.7	4.0	16.8	94
SVM		7.0	3.5	2.9	14.5	741
kNN		18.9	13.2	11.8	25.9	750
Gauss		6.8	3.2	**2.6**	**14.2**	18
MLP_ReLU	PCA	23.2	25.1	16.3	28.9	72
MLP_TanH		33.7	32.0	19.7	28.8	92
SVM		46.1	45.8	42.6	**28.2**	1,853
kNN		25.8	25.5	19.3	32.3	868
Gauss		22.9	21.5	**16.0**	30.6	22
MLP_ReLU	3-Band	8.8	10.8	9.2	23.8	71
MLP_TanH		16.2	17.9	16.1	24.7	91
SVM		14.7	14.8	14.0	23.0	1797
kNN		11.5	7.6	**7.3**	**22.5**	40,988
Gauss		23.4	23.2	22.9	29.9	21

Table 1: $Error_{disease}$ percentage of *Alternaria* vs. Ozone and $Error_{damage}$ percentage of Damaged leaf vs. Healthy leaf. Time is measured during testing.

because of its much higher classification speed (71 ms). Also MLP_ReLU seems to always be faster than MLP_TanH.

Results of the damage classifier for using 3 wavelengths show relatively high error rates (22.5%). The best error rate for damage detection is produced by using all wavelengths and an SVM (13.4%). The speed difference between SVM and MLP is mainly because the SVM uses a single core CPU implementation and the MLP uses a GPU implementation.

4 Discussion and Future work

A hyper-spectral image cube of 28 wavelengths has been recorded to classify between Healthy leaf, *Alternaria* damage and ozone damage. Increasing patch size generally leads to lower pixel-classification error rates. Using an MLP with a ReLU activation function shows the best result. Especially when taking classification speed into account (and high sample counts).

Surprisingly the results show that detecting damaged leaves is more difficult for the classifiers than distinguishing between *Alternaria* and Ozone (13.4% vs. 1.5%). This is probably because of the subtle color difference in the outer ring of *Alternaria* lesions, compared to the leaf.

LDA shows to be an excellent dimensionality-reduction method. Reducing

ESANN 2017 proceedings, European Symposium on Artificial Neural Networks, Computational Intelligence and Machine Learning. Bruges (Belgium), 26-28 April 2017, i6doc.com publ., ISBN 978-287587039-1. Available from http://www.i6doc.com/en/.

the dimensions from 700 to 2 only increases errors from 1.5% to 2.6%. Error rates increase to 7.3% when selecting the 680nm, 520nm and 540nm wavelengths. This final result shows that a camera system on a UAV can be used with three high-resolution cameras and three optical filters. This is preferable to a hyper-spectral camera system because of payload constraints, imaging resolution and cost.

In the future some kind of majority voting of image pixels can be used to classify individual leaves. The next step is to use a UAV to record more images of potato leaves using the three selected wavelengths and to use deep learning to detect diseases.

Acknowledgments

The dataset was collected within the RAAK SIA Smart Vision for UAVs project. HLB B.V. contributed potato leafs with the ground-truth per leaf.

References

[1] Sally Wilkinson, Gina Mills, Rosemary Illidge, and William J Davies. How is ozone pollution reducing our food supply? *Journal of Experimental Botany*, 63(2):527–536, 2012.

[2] L. J. Turkensteen, J. Spoelder, and A. Mulder. Will the real Alternaria stand up please: Experiences with Alternaria–like diseases on potatoes during the 2009 growing season in The Netherlands. *PPO-Special Report no. 14. Proc. 12th EuroBlight Workshop. France*, pages 165 – 170, 2010.

[3] J. van de Loosdrecht, K. Dijkstra, J. H. Postma, W. Keuning, and D. Bruin. Twirre: Architecture for autonomous mini-UAVs using interchangeable commodity components. In *IMAV 2014: International Micro Air Vehicle Conference and Competition*. Delft University of Technology, 2014.

[4] Jesper Rasmussen, Georgios Ntakos, Jon Nielsen, Jesper Svensgaard, Robert N. Poulsen, and Svend Christensen. Are vegetation indices derived from consumer-grade cameras mounted on UAVs sufficiently reliable for assessing experimental plots? *European Journal of Agronomy*, 74:75–92, 2016.

[5] Julien Rebetez, Héctor F. Satizábal, Matteo Mota, Dorothea Noll, Lucie Büchi, Marina Wendling, Bertrand Cannelle, Andres Perez-Uribe, and Stéphane Burgos. Augmenting a convolutional neural network with local histograms - a case study in crop classification from high-resolution UAV imagery. In *ESANN 2016 proceedings, European Symposium on Artificial Neural Networks, Computational Intelligence and Machine Learning*, 2016.

[6] Sharada P. Mohanty, David P. Hughes, and Marcel Salathé. Using deep learning for image-based plant disease detection. *Frontiers in Plant Science*, 7:1419, 2016.

[7] W. N. Venables and B. D. Ripley. *Modern Applied Statistics with S*, volume Fourth edition. Springer, 2002.

[8] Chih-Chung Chang and Chih-Jen Lin. LIBSVM: A library for support vector machines. *ACM Transactions on Intelligent Systems and Technology*, 2:27:1–27:27, 2011.

[9] Yangqing Jia, Evan Shelhamer, Jeff Donahue, Sergey Karayev, Jonathan Long, Ross Girshick, Sergio Guadarrama, and Trevor Darrell. Caffe: Convolutional architecture for fast feature embedding. *arXiv preprint arXiv:1408.5093*, 2014.

[10] Alex Krizhevsky, Ilya Sutskever, and Geoffrey E. Hinton. Imagenet classification with deep convolutional neural networks. In F. Pereira, C.J.C. Burges, L. Bottou, and K.Q. Weinberger, editors, *Advances in Neural Information Processing Systems 25*, pages 1097–1105. Curran Associates, Inc., 2012.